# Giant second-harmonic generation in a one-dimensional GaN photonic crystal

J. Torres, D. Coquillat,* R. Legros, J. P. Lascaray, F. Teppe, D. Scalbert, D. Peyrade, Y. Chen, O. Briot, M. Le Vassor d'Yerville, E. Centeno, D. Cassagne, and J. P. Albert

*Groupe d'Etude des Semiconducteurs, UMR 5650, CNRS-Université Montpellier II, pl. E. Bataillon, 34095 Montpellier, France and Laboratoire de Photonique et des Nanostructures, CNRS UPR 20, Route de Nozay, 91460 Marcoussis, France*

(Received 8 July 2003; revised manuscript received 8 October 2003; published 20 February 2004)

In order to determine the angular geometry that satisfies quasi-phase matching conditions for enhanced second-harmonic generation (SHG), the equi-frequency surfaces of the resonant photonic modes (that lie above the light line) of a one-dimensional GaN photonic crystal have been experimentally and theoretically studied as a function of frequency, angle of incidence, and azimuthal direction. Enhancement of the SHG has been observed when the angular configuration satisfies the quasi-phase matching conditions, i.e., when both the fundamental and second-harmonic fields coincide with resonant modes of the photonic crystal. The SHG enhancement achieved to the double resonance was 5000 times with respect to the unpatterned GaN layer. A smaller, but still substantially enhanced SHG level was also observed when the fundamental field is coupled into a resonant mode, while the second-harmonic field is not.

DOI: 10.1103/PhysRevB.69.085105 PACS number(s): 42.70.Qs, 42.65.Ky, 78.66.Fd

## I. INTRODUCTION

Photonic crystals (PhCs) have attracted widespread interest in recent years because of their ability to alter the dispersion relations of photons.[1–3] Among the many practical applications which are likely to be found for the unique optical properties of PhCs, one of the most exciting issues resides in the possibility of obtaining a large enhancement in the nonlinear optical response.[4]

In the case of noncentrosymmetric crystals with significant second-order nonlinear coefficients, the phase-matching conditions for processes such as second-harmonic generation (SHG) are not normally fulfilled because of material dispersion. This problem can be solved however by using periodically modulated materials.[5–10] In this case it is the periodicity which provides the phase matching conditions for the incident and generated beam. This mechanism is called quasi-phase matching (QPM)[11,12] and takes into account the reciprocal lattice vectors of the periodic structure to compensate for the wave vector mismatch in situations where direct phase matching is not possible. Furthermore, PhCs high refractive index contrast contribute to the SHG enhancement in two ways: not only do they make it possible to satisfy the QPM conditions, but the strong spatial confinement of the fundamental and second-harmonic (SH) fields can enhance the nonlinear response considerably.[8] Previous reports have demonstrated that efficient SHG can be achieved in one-dimensional PhCs.[8,9,13,14]

PhCs in planar geometry can support two kinds of modes classified according to their position with respect to the light line: (i) purely guided bound modes that are completely confined inside the waveguide, without any coupling to external radiation; these modes lie below the light line of the cladding material; (ii) resonant modes also termed quasi-guided modes,[15,16] located in the vicinity of the waveguide; the latter modes lie above the light line and possess in-plane Fourier components which can be phase-matched to external radiation. Cowan and Young recently reported in Ref. 17 a calculation showing that the SH conversion efficiency can in principle be enhanced by up to six orders of magnitude when both the fundamental and the SH fields are coupled into such resonant modes. In this case the QPM condition is written as[17]

$$\Delta \mathbf{k} = \mathbf{k}_{\parallel}(2\omega) - 2\mathbf{k}_{\parallel}(\omega) \pm \mathbf{G} = 0, \tag{1}$$

where $\mathbf{k}_{\parallel}(\omega)$ and $\mathbf{k}_{\parallel}(2\omega)$ refer to the in-plane wave vectors of the resonant fundamental mode at $\omega$ and of the resonant SH mode at $2\omega$, respectively, while $\mathbf{G}$ is a reciprocal lattice vector. Because these QPM conditions might occur away from the high-symmetry directions, it is then essentially important to consider the *full* photonic band structure of the PhC.

Although the strong confinement of both the fundamental and the SH fields has been shown to play a decisive role in SHG enhancement,[8] experimental SHG enhancement has so far been observed when only the fundamental field is confined.[7,18]

To obtain efficient SHG, a nonlinear material with high nonlinear coefficients is required. Nitrides are attractive materials for optical wavelength conversion[19] with second-order susceptibility $\chi^{(2)}$ comparable to conventional nonlinear crystals such as KDP or $LiNbO_3$, a wide electronic bandgap (without absorption either of the fundamental wave in the near infrared or of the second-harmonic in the near UV), and a high optical damage threshold. Nevertheless, the efficiency of the SHG in bulk GaN is too low for practical applications[19,20] because GaN is a highly dispersive material. Appropriate PhC structures patterned in GaN on sapphire waveguides should provide the flexibility required to fulfill QPM conditions and enable much higher conversion efficiency. We have previously reported band-structure measurements of two-dimensional PhC structures realized in GaN on sapphire samples[21–23] as well as measurements of their photoluminescence properties.[24,25]

The *full* band diagram for all $k$ wave vectors in the first Brillouin zone (not only along the high symmetry directions) has been also calculated or experimentally investigated in

 

various PhCs.[26–37] However only linear optical properties were considered in these works whose major aim was to explain anomalous propagation phenomena by analyzing the shapes of the equi-frequency surfaces (EFS) of the photonic bands.

In this paper we demonstrate the giant enhancement of SHG in a one-dimensional (1D) GaN PhC structure caused by the simultaneous confinement of both fundamental and SH fields which occurs when the QPM conditions [Eq. (1)] are fulfilled. First, we have studied, experimentally as well as numerically, the linear dispersion properties of the resonant modes that characterize the 1D-GaN PhC for various polar and azimuthal directions. The theory based on a rigorous scattering matrix method[38] has provided a good description of the photonic bands and of the EFS and has enabled us to construct the EFS for the frequencies unavailable experimentally. We shall then show that the EFS may be used to identify the angular configurations in which QPM conditions [Eq. (1)] can be satisfied. The SH intensity from the 1D-GaN PhC is then recorded as a function of the wavelength and azimuthal angles, for a fixed angle of incidence. A giant SHG enhancement was achieved due to simultaneous spatial localization of the both fields, while a smaller, but still substantially enhanced, SHG level was also observed when only the fundamental field is phase matched with a resonant mode, while the SH field is not.

## II. SAMPLE AND SETUPS

A thin GaN epitaxial layer was grown by metalorganic vapor phase expitaxy on the (0001) surface of a sapphire substrate with the $c$ axis of the GaN crystal normal to the surface. A 1D GaN PhC structure was fabricated by techniques described in Ref. 39 in the 260-nm-thick GaN layer. The unpatterned GaN layer forms a monomode waveguide at a wavelength of 791 nm and supports three guided modes at 395.5 nm. The refractive index of GaN is $n=2.345$ at 791 nm and $n=2.546$ at 395.5 nm. The PhC structure consists of a succession of air-GaN stripes with a periodicity of $a=500$ nm over a patterned area of $500\times500\ \mu\mathrm{m}^2$. The stripe depth was estimated using atomic force microscope measurements to be 230 nm. The stripe sidewalls are not exactly vertical, and the air-filling factor varies over the $z$ extension of the PhC. The average air-filling factor was estimated to be 0.20. The wurtzite structure of GaN belongs to the 6 mm point group symmetry; then the three nonzero tensor elements of the second-order susceptibility $d_{15}$, $d_{31}$, and $d_{33}$ are therefore responsible for the SHG. These tensor coefficients are related to each other as $d_{15}\approx d_{31}$ and $d_{33}/d_{31}\approx-2$ while the measured value of $d_{33}$ is $-4.5$ pm/V.[19] GaN films on sapphire having their $c$ axis normal to the surface are optically uniaxial and thus SHG is suppressed at normal incidence. However by increasing the angle of incidence $\theta$ up to roughly 55°, $p-p$ ($p$-polarized incident fundamental beam and $p$-polarized SH signal) and $s-p$ ($s$-polarized incident fundamental beam and $p$-polarized SH signal) polarization measurements of the SHG intensity are observed to increase and to be independent of the azimuthal orientation of the sample.[40] Therefore, for a given fundamental wavelength and polarization, the SHG intensity is dependent on the layer thickness and on the angle of incidence of the fundamental beam only. Consequently the GaN film and the PhC can have arbitrary orientations in contrast to a GaAs film.[41,18]

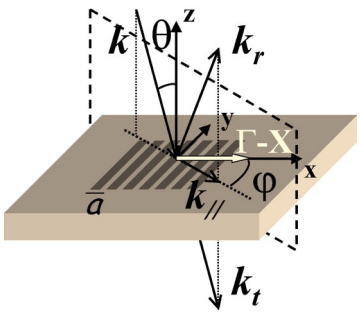


FIG. 1. Schematic diagram illustrating the 1D GaN PhC in planar waveguide geometry, and the coordinate system used in this study. Here $a$ is the periodicity of the PhC.

Our SHG measurements were conducted in two steps. First, the characterization of the photonic band structure, or dispersion relation $\omega(k)$, was carried out using an angularly resolved transmission and reflection surface coupling technique.[42–45,35,22,16,46] In this technique the 1D PhC is used to couple incident light into the resonant modes. The periodicity of the dielectric here provides the necessary in-plane wave vector enhancement via a reciprocal lattice vector $\mathbf{G}$. That is, in the plane of the PhC:

$$\mathbf{k}_{\mathrm{RM}}(\omega)=\mathbf{k}_{\parallel}(\omega)\pm\mathbf{G}. \tag{2}$$

Here $\mathbf{k}_{\mathrm{RM}}(\omega)$ and $\mathbf{k}_{\parallel}(\omega)$ denote the in-plane wave vectors of the resonant mode and the incident field, respectively. We have observed the zero-order transmission and reflection spectra (in this case $\mathbf{G}=0$) for collimated broad-spectrum light incident on the surface of the PhC over a range of incidence and azimuthal angles. The local coordinate system which is used here is illustrated in Fig. 1. The incident wave vector $\mathbf{k}(\omega)$, together with the $z$ axis normal to the PhC plane, defines the plane of incidence. The direction of the wave vector $\mathbf{k}(\omega)$ is specified by the angle of incidence $\theta$ between $\mathbf{k}(\omega)$ and the $z$ axis ($|\mathbf{k}_{\parallel}(\omega)|=|\mathbf{k}(\omega)|\sin\theta$), and by the azimuthal angle $\varphi$ between the in-plane wave vector $\mathbf{k}_{\parallel}(\omega)$ and the direction perpendicular to the stripes. The sample holder was mounted on two rotary stages which allow $\theta$ to vary from 0° to 55° and $\varphi$ from 0° to 90°. The orientation of the PhC was determined from the diffraction pattern: if all the diffracted beams lie in the plane of incidence, then $\varphi$ is set equal to zero. The beam divergence was estimated to be $\Delta\theta\approx2°$. The polarization of the incident light was selected to be either $s$ or $p$ by using a prism polarizer. Transmission and reflection spectra were acquired with a Fourier-transform spectrometer over two spectral ranges: the visible-near IR range 450 nm–1.1 $\mu$m, with a spectral resolution of 4 $\mathrm{cm}^{-1}$ (0.8 nm at 500 nm), and the near IR range 833 nm–2.5 $\mu$m with a spectral resolution of 8 $\mathrm{cm}^{-1}$ (0.8 nm at 1 $\mu$m). This experiment makes it possible to measure the topology of the photonic band structure of the resonant modes. Each band is then represented by a surface. The

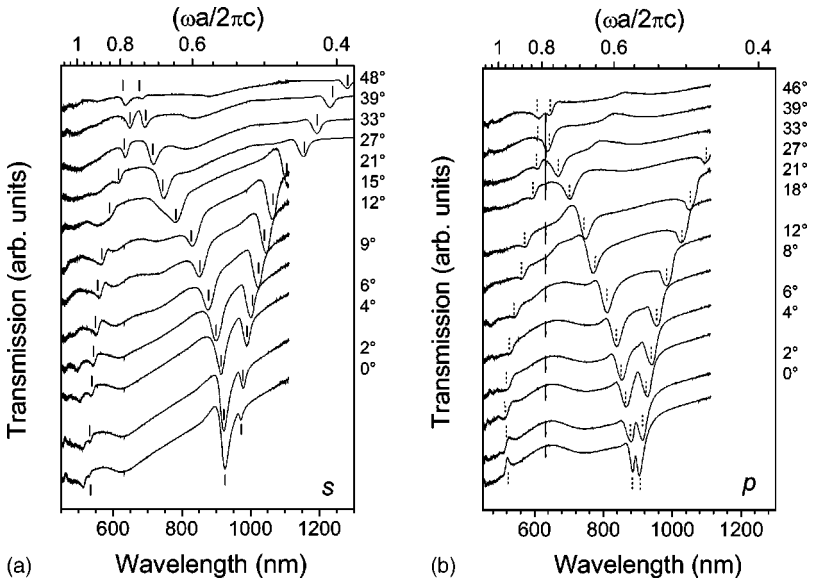


FIG. 2. Experimental incidence-angle $\theta$ dependent transmission spectra along the $\Gamma-X$ direction, i.e., perpendicular to the stripes ($\varphi=0°$) with (a) *s*- and (b) *p*-polarized light. Solid (dotted) vertical bars mark the resonances arising from coupling to *s* (*p*) resonant Bloch modes. The feature at 632.8 nm observed for the two polarizations is due to the HeNe laser used to control the position of the mirror of the FTIR spectrometer.

EFS are obtained by the intersection of these surfaces and the horizontal plane associated with a constant value of the frequency $\omega$.

Second, a femtosecond titanium:sapphire laser pumped by a frequency doubled YAG laser was used as source (fundamental beam) to investigate the SHG in the 1D GaN PhC. The wavelength of the source could be varied continuously in the range 720–850 nm and had a measured full width at half maximum intensity (FWHM) of 15 nm. At the repetition rate of 82 MHz, the energy per pulse was 10 nJ. The *s*-polarized fundamental beam was weakly focused on the sample surface by a 10 cm focal-length lens that produced a focal-spot less than 80 $\mu$m in diameter. The corresponding pump pulse intensity $I(\omega)$ was approximately equal to 1 GW/cm$^2$. The intensity $I_R(2\omega)$ of the zero-order diffracted SH beam was measured in a reflection geometry and a highly nonlinear crystal (BBO) was used as reference to align the system; the direction of the zero-order diffracted SH beam then coincides with that of the zero-order reflected fundamental beam. These two beams were separated by an Amici prism and the SH signal was dispersed by a 0.60 m monochromator using a 1200 grooves/mm grating and a slit width of 600 $\mu$m. Detection was performed with an UV enhanced photomultiplier. In order to express the SH generated by the PhC in absolute units, the radiation emitted by the BBO crystal was filtered to eliminate the fundamental frequency and successively directed to a power meter for measuring the average output power and to the neutral filter/spectrometer/photomultiplier tube combination. The SH response from the PhC was then measured using the spectrometer/photomultiplier tube combination using an identical slit width and compared with the SH signal generated by the BBO crystal.

The wavelength range of the laser beam allows coupling into the second lowest resonant mode. The SHG intensity was recorded by varying the wavelength, the angle $\theta$, and by tuning $\varphi$. In this experimental configuration, $\varphi=0°$ again corresponds to propagation along the $\Gamma-X$ direction. The SH intensity was then compared with that obtained on the unpatterned GaN layer near the PhC, under the same angular and polarization conditions in order to specifically characterize the contribution of the PhC in the nonlinear conversion.

## III. LINEAR PROPERTIES: EQUIFREQUENCY SURFACES

Figures 2(a) and 2(b) show typical angular resolved transmission spectra obtained for the 1D GaN PhC for *s*- and *p*-polarized incident light, respectively, with the plane of incidence aligned along the $\Gamma-X$ direction. The resonance features visible in the spectra correspond to the coupling of the incident beam into the resonant modes. When $\theta$ was increased from 0° up to 50°, these resonances were clearly observed to disperse. Along the $\Gamma-X$ symmetry direction the modes can be excited selectively by using either *s*- or *p*-polarized light and can thus be labeled accordingly. For propagation directions away from $\Gamma-X$, these two polarizations are mixed and modes radiate an elliptically polarized field.[45] However in the following text, for convenience in their labeling, the modes will be referred to as *s* or *p* by continuity according to their polarization at $\varphi=0°$. In transmission (reflection) measurements, we have chosen the *minima* (*maxima*) as the wavelength positions of the excited resonant modes.

Figures 3(a) and 3(b) show typical azimuthal-angle dependent $\varphi$ reflection spectra for a fixed value of $\theta=44°$ when the plane of incidence twists away from the $\Gamma-X$ direction over the $\varphi$ range from 0° to 90°. For azimuthal orientations $\varphi\neq0°$, the symmetry is broken and the polarization of the reflected signal at the resonance wavelengths is elliptic. The evolution of the resonances from $\varphi=0°$ to 90° shows progression of the polarization mixing; the light incident as $s(p)$ can emerge at the resonances wavelengths with a $p(s)$ polarization component due to the polarization rotation[47,36] [Figs. 3(a) and 3(b)]. Hence, the 1D PhC may be used to couple an $s$-($p$-) polarized beam to a resonant mode identified as $p(s)$ at $\varphi=0°$.

A plot of the frequency positions of the resonances as a

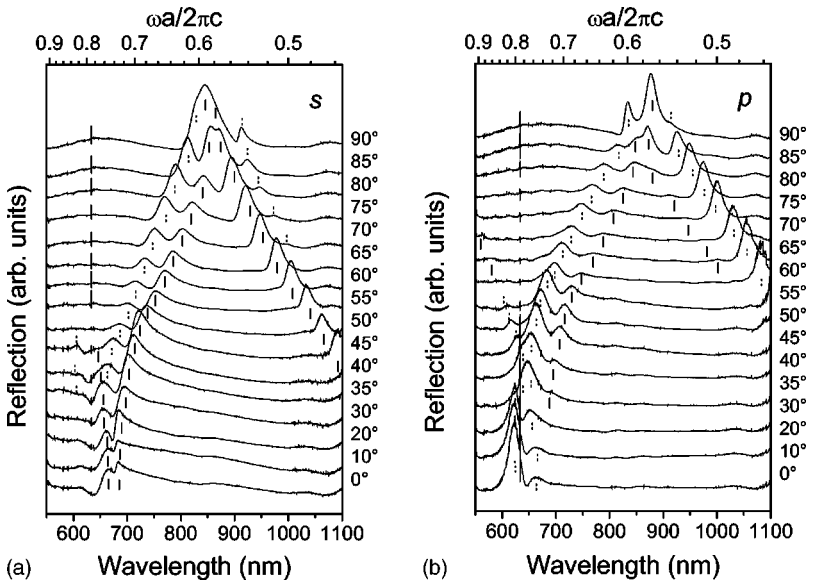


FIG. 3. Typical azimuthal-angle $\varphi$ dependent experimental reflection spectra with incident light at fixed angle of incidence of $\theta=44°$ for (a) *s*- and (b) *p*-polarized light. $\varphi$ varies from 0° ($\Gamma-X$ direction) to 90°. Along the $\Gamma-X$ symmetry direction the modes are excited by either *s*- or *p*-polarized light. For propagation directions away from $\Gamma-X$, these two polarizations are mixed and modes radiate an elliptically polarized field. For convenience in their labeling, the modes are referred to as *s* or *p* by continuity according to their polarization at $\varphi=0°$. Solid (dotted) vertical bars mark the resonances arising from coupling to *s*- (*p*-) labeled resonant Bloch modes. The feature at 632.8 nm observed for both polarizations is due to the HeNe laser used to control the position of the mirror of the FTIR spectrometer.

function of the in-plane wave-vector values along the $\Gamma-X$ symmetry direction is given in the diagrams of Figs. 4(a) and 4(b) for *s* and *p* polarization, respectively. The heavy-solid lines represent the air light-lines, delimiting the range of wave vectors accessible by an incident photon from the air-side.

A scattering matrix method[38] was used to model the experimental dispersion curves and to obtain the band structure in the wavelength region unavailable experimentally. The calculation contains all the information related to the etched photonic structure, such as refractive indices (the frequency dispersion of the refractive indices of GaN and sapphire are taken into account by calculating each band with appropriate values of refractive indices taken at an average frequency), layer thickness (260 nm), and etch depth (230 nm). The Fourier transform of the inverse of the dielectric constant was modeled according to Ref. 48 and 109 plane waves were used in the calculations. The nonverticality of the walls due to the etching process has been taken into account via an effective air-filling factor considered as a fitting parameter. For the two lowest resonant modes a good agreement with the experimental results was achieved by using an effective air-filling factor equal to 0.20. As can be seen from the figures, small quantitative discrepancies still remain for the third mode. This could be related to the experimental uncertainty in the determination of the values of $\theta$ and $\varphi$ angles, to the energy position estimation for the Fano-shaped experimental resonances, and to the shape of the holes. Note that the first band of the photonic band structure [not shown in Figs. 4(a) and 4(b)] is a guided mode. The second band, above the light cone, corresponds to the lowest resonant mode.

Keeping the same value for the filling factor parameter, the construction of the corresponding EFS can be obtained numerically.

Figure 5 illustrates in a polar reciprocal-space, as a function of the azimuthal angle $\varphi$, the experimental and calculated EFS corresponding to the second-lowest resonant mode

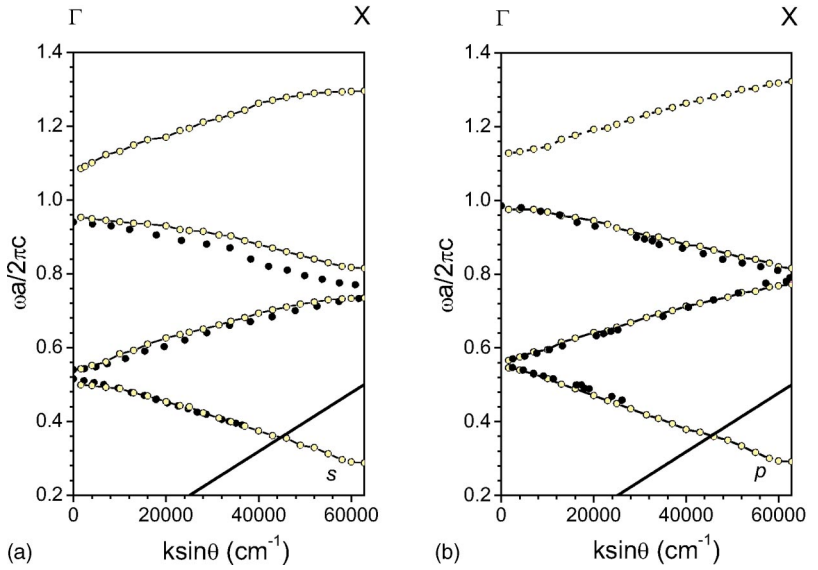


FIG. 4. Photonic band structure of the GaN PhC for (a) *s*- and (b) *p*-polarized light as determined from the incidence-angle $\theta$ dependent transmission spectra (closed dots) and from theoretical calculation (solid lines and open dots) for incidence plane along the $\Gamma-X$ direction.

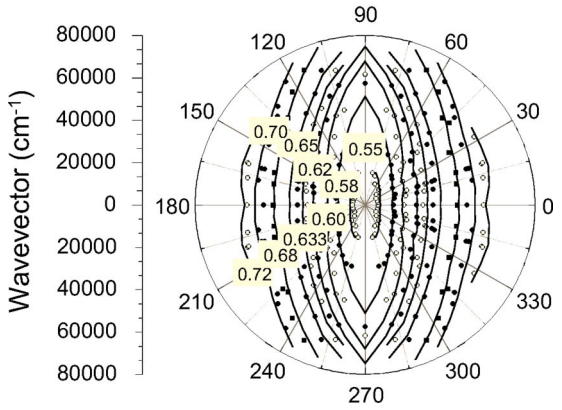


FIG. 5. Experimental EFS (the different EFS are one after another represented with closed or open dots to better appreciate their evolution) for the second resonant mode compared with theoretically calculated results (solid lines). Incident light is *s*-polarized with $0.55 \leqslant \omega a/(2\pi c) \leqslant 0.72$. Data and calculations have been obtained between $\varphi = 0°$ and $\varphi = 90°$, and reflected about the *x* and *y* axes to produce the full 360° polar map.

for various frequencies ($0.55 \leqslant \omega a/2\pi c \leqslant 0.72$) and for *s*-polarized incident light. In this representation, $k_x = |\mathbf{k}| \sin\theta \cos\varphi$ and $k_y = |\mathbf{k}| \sin\theta \sin\varphi$. Data have been recorded in transmission by varying $\varphi$ between 0° and 160°. The EFS are labeled *s* or *p* considering whether the mode is excited either *s* or *p* at $\varphi = 0°$. These EFS describe ellipses in polar reciprocal space, the long axes of which are aligned in the direction of the *y* ($\varphi = 90°$) axis (Fig. 5). However these ellipses are clearly deformed near the *X* point, an effect that can be attributed to an increased band mixing around the high symmetry points, close to the band-edge.[33]

Figure 6 shows the EFS for the second-resonant mode at 791 nm [$\omega a/(2\pi c) = 0.632$] when *p*-polarized and *s*-polarized incident beams were used for excitation. The solid curves report the results of the numerical calculations, which are found to be in excellent agreement with the experimental data. This demonstrates that our calculation procedure, which uses only one free parameter determined by fitting the two lowest bands in the $\Gamma - X$ direction, is able to reproduce accurately the 1D GaN PhC bands along any direction in the whole range $0.4 \leqslant \omega a/(2\pi c) \leqslant 1.0$. This gives us some confidence in the construction of the EFS for higher lying modes for which the experimental resonances are in a wavelength range unavailable for our angular resolved transmission and reflection measurement set-up ($\omega a/(2\pi c) \geqslant 1.0$).

## IV. EXPERIMENTAL SECOND-HARMONIC GENERATION

By using the calculated EFS, it is possible to identify the geometrical configurations which will allow QPM to be satisfied and observed experimentally in the available wavelength range of the laser. In addition we have chosen a wavelength value which fulfilled a QPM condition at $\theta$ around 45° for which the SHG response of the unpatterned GaN layer is sufficient. A wavelength of 791 nm satisfied such a requirement. Actually in the case of zero-order diffracted beam the phase-mismatch is given as

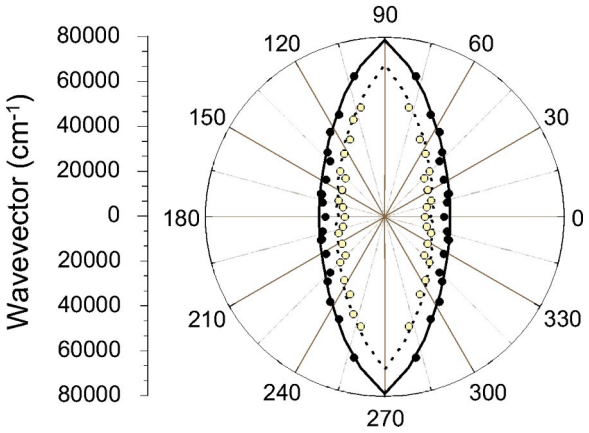


FIG. 6. Experimental and calculated EFS for the second-resonant mode at $\omega a/(2\pi c) = 0.632$ ($\lambda = 791$ nm). Experimental: closed (open) dots for *s*- (*p*-) polarized incident light. Calculated: solid (dashed) lines for *s*- (*p*-) polarized incident light. The excellent agreement between experimental data and calculations gives us some confidence in the construction of EFS for higher-lying modes for which wavelength range is unavailable for our experimental setup.

$$\Delta\mathbf{k} = \mathbf{k}_{\parallel}(2\omega) - 2\mathbf{k}_{\parallel}(\omega). \tag{3}$$

The comparison of the calculated EFS at $\omega$ and $2\omega$ allows the determination of the QPM conditions under which $|\Delta\mathbf{k}| = 0$ is satisfied. Solid lines in Fig. 7 represent the calculated EFS at 791 nm (EFS labeled *s* is in-filled circles, and *p* in-filled squares) with which the fundamental field can be phase matched. In a similar manner dashed lines indicate EFS calculated at 395.5 nm (EFS labeled *s* is in open circles, and *p* in open squares) and plotted at half their frequency and in-plane wave vector,[17] with which the SH field can be phase matched. The large circles in Fig. 7 indicate points where the absolute value of $|\Delta\mathbf{k}|$ reaches zero. The QPM conditions

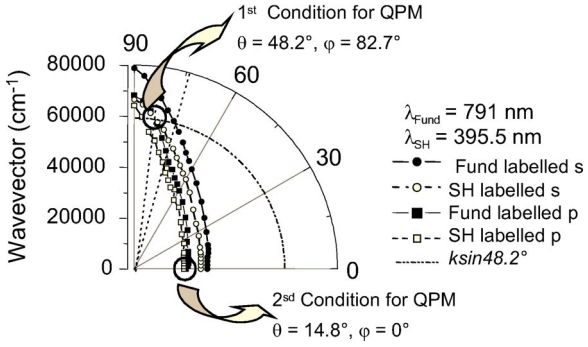


FIG. 7. Calculated EFS at fundamental wavelength 791 nm [$\omega a/(2\pi c) = 0.632$] and at SH wavelength 395.5 nm [$\omega a/(2\pi c) = 1.264$, plotted at half its in-plane wave vector] for *s*- and *p*-polarized incident light. Fundamental: *s*-polarized (closed circles), *p*-polarized (closed squares). SH: *s*-polarized (open circles) *p*-polarized (open squares). Circles indicate two coincidence points ($\theta = 48.2°$, $\varphi = 82.7°$) and ($\theta = 14.8°$, $\varphi = 0°$) where the QPM should occur. The dashed-dotted quarter circle represents the extremity of the in-plane wave vector $|\mathbf{k}(\omega)| \sin\theta$ with $\theta = 48.2°$, while $\varphi$ is tuned from 0° to 90°.

should be satisfied for two geometrical configurations: (i) when the EFS labeled *p* for the fundamental field crosses the EFS labeled *s* for the SH field ($\theta=48.2°$ and $\varphi=82.7°$) and (ii) when the EFS labeled *p* for the fundamental field crosses the EFS labeled *p* for the SH field ($\theta=14.8°$ and $\varphi=0°$). In unpatterned GaN films, the SH signal is much greater for $\theta=48.2°$ than for $\theta=14.8°$, so we chose to investigate SHG at $\theta$ close to 48.2°. The dashed-dotted quarter circle in Fig. 7 represents the extremity of the in-plane wave vector $|\mathbf{k}(\omega)|\sin\theta$ with $\theta=48.2°$, while $\varphi$ is tuned from 0° to 90°. The dashed-dotted quarter circle intersects the EFS labeled *s* for 791 nm at $\varphi=74°$. In this geometrical configuration, the fundamental field alone is efficiently confined and the QPM is not achieved.

Experimentally the variation of the SHG intensity may be measured by scanning either the fundamental wavelength or the incidence and azimuthal angles. Keeping the angle of incidence constant avoids the difficulty of changing dramatically the optical path of the SH generated signal. This latter procedure has thus been adopted in this work.

The azimuthal angle $\varphi$ was tuned to obtain the maximum efficiency at the fundamental beam wavelength of 791 nm. According to the band structure diagrams this fundamental beam which was *s*-polarized can then match the second lowest resonant modes, labeled either *p* or *s*. Figure 8 shows the reflected SHG intensity as a function of the azimuthal angle $\varphi$ at fixed incidence angle $\theta=44°$. The results have been normalized against the SH signal from the unpatterned GaN layer illuminated under identical conditions. The SHG angular spectrum shows two sharp peaks at 83° and 98° and a broad peak at 69°. A comparison with the angular representation of the EFS (Fig. 7) makes it possible to associate the sharp maximum at 83° with the achievement of the QPM condition at the crossing between the *p*-resonance fundamental wavelength (closed squares) and the *s*-resonance SH wavelength (open circles). The resulting SH intensity at the QPM conditions is more than 5000 times the inherent value for GaN. The peak at 98° is symmetrical with that at 83° with respect to the angle $\varphi=90°$ such as the QPM conditions are again observed. On the other side the broad peak at 69° is due to the sole confinement of the fundamental field in the vicinity of the resonant mode labeled *s* (intersection between the dashed-dotted quarter circle and the EFS represented by closed circles in Fig. 7). As a result, the SHG is increased by a factor of approximately 350. Away from the resonant interaction conditions, in the ranges of $\varphi$ from 85° to 95° and from 52° to 62°, the SHG signal is similar with that for GaN regions adjacent to the PhC.

When both confinement (fundamental and harmonic) mechanisms occur the SHG signal magnitude is found to be approximately 15 times higher and the FWHM is a factor of 2 narrower when compared with the SHG enhancement achieved with the sole confinement of the fundamental field. This clearly demonstrates the combined roles of the fundamental and SH fields confinement in the enhancement of the SHG signal from the 1D PhC.

Figure 9 represents the SH pulse intensity $I_R(2\omega)$ generated when the QPM conditions are satisfied (*s*-polarized fundamental beam, with $\theta=44°$ and $\varphi=83°$) as a function of the beam pulse intensity. As expected, the curve follows a quadratic behavior. The nonlinear reflection coefficient defined as $R_{\mathrm{NL}}=I_R(2\omega)/I(\omega)^2$ was estimated to be greater than $4.3\times10^{-22}\,\mathrm{m^2\,W^{-1}}$. This nonlinear reflection coefficient is nearly two orders of magnitude better than the nonlinear reflection coefficient achieved in Ref. 18 for a GaAs PhC when the fundamental field alone is phase matched with a resonant mode. Note that for subpicosecond pulses, the enhancement is strongly reduced due to the broad frequency content of the pulse. Furthermore, we have shown in Fig. 7

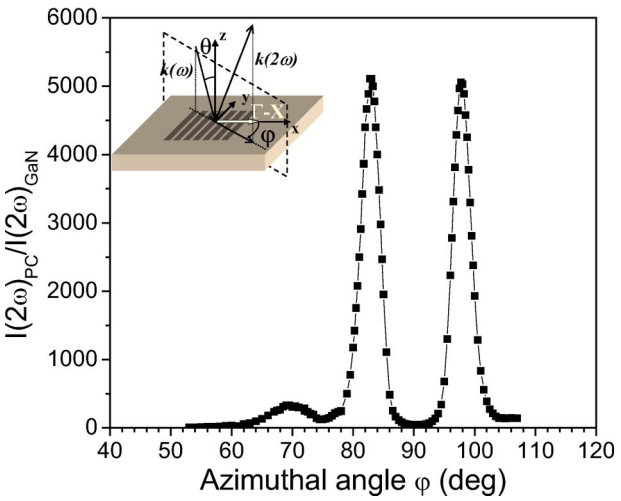


FIG. 8. SH intensity generated by a fundamental beam at $\theta=44°$ inside the one-dimensional GaN PC, measured in reflection geometry as a function of the azimuthal rotation angle $\varphi$. The fundamental wavelength is 791 nm and is *s*-polarized. The SH signal was normalized against the SH signal of the unpatterned GaN layer for each azimuthal angle. The line connecting the experimental data points is a guide for the eye. The fundamental beam was *s*-polarized, however due to the polarization mixing for $\varphi\neq0°$ the fundamental beam can be resonant with a *p*-polarized mode. Inset: Experimental configuration where the zero-order diffracted SH signal is collinear with the specular reflected fundamental beam.

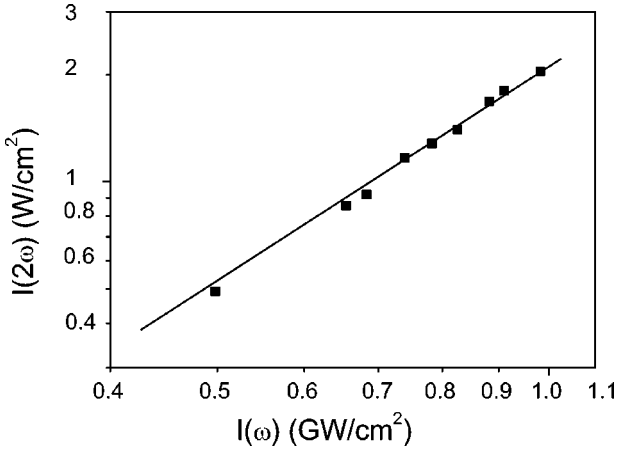


FIG. 9. The pulse intensity of the SH as a function of the pulse intensity of the fundamental incident onto the PhC. The fundamental beam was *s*-polarized, $\theta=44°$ and $\varphi=83°$. The squares represent the measured points and the solid line is a quadratic fit.

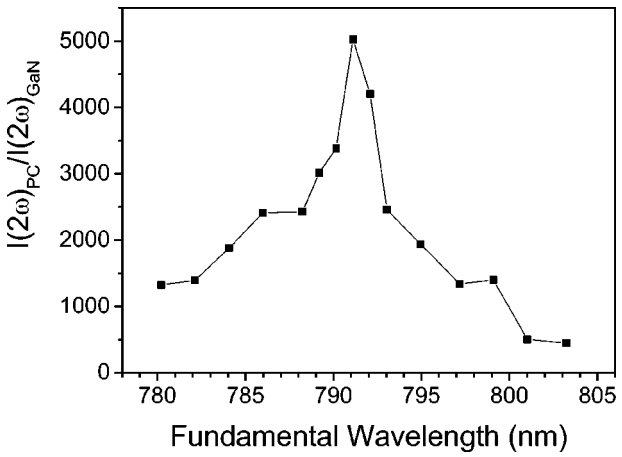


FIG. 10. SH intensity normalized against the SH signal of the unpatterned GaN layer as a function of the fundamental wavelength. The fundamental beam is *s*-polarized and the incidence and azimuthal angles are $\theta=44°$ and $\varphi=83°$, respectively. The line connecting the experimental data points is a guide for the eye.

that a second QPM condition might be fulfilled for $\theta=14.8°$ and $\varphi=0°$, i.e., along the $\Gamma-X$ direction for which polarization mixing is absent. Hence, a larger enhancement in the SH should occur at the predicted $p-p$ SHG process.

The SH intensity normalized to the unpatterned GaN layer as a function of the fundamental wavelength is shown in Fig. 10 at $\theta=44°$ and $\varphi=83°$. The observed dependence is dominated by the enhancement due to the QPM condition at 791 nm, superimposed on a signal due to the broad spectral FWHM of the laser beam, together with the FWHM of the relevant resonances for the fundamental and SH fields.

The angular configuration at the maximum SHG point ($\theta=44°$ and $\varphi=83°$) obtained from the nonlinear experiments agrees closely with QPM conditions ($\theta=48.2°$ and $\varphi=82.7°$) determined beforehand from the EFS in Fig. 7. The slight departure can be attributed to (i) the small differences, observed for example in Figs. 4(a) and 4(b) between experimental and calculated photonic band structure, (ii) the angle of incidence step of either 2 or 3 degree for both linear and nonlinear measurements which add directly to the inaccuracy of the result, (iii) the accumulated errors in angular measurements (position of zero for $\theta$ and $\varphi$).

Comparison with previous theoretical studies by Cowan and Young in Ref. 17 shows that the magnitude of the SHG enhancement obtained in our investigations is approximately one- to two-orders-of-magnitude smaller. However, for this particular 1D GaN PhC, the enhancements have not yet been optimized. Especially, the availability of resonant modes with strong fundamental and SH fields overlap could lead to a greater enhancement of SHG. Moreover, Cowan *et al.*[17] have shown clearly how the SH response is strongly influenced by the quality factor $Q$ of the resonant modes which allow one to accumulate large local field in the vicinity of the PhC surface. Therefore, a way for further improvement is the engineering of the quality factor of the relevant modes for the future photonic structures. The efficiency of SHG should be increased by taking advantage of the piezoelectric field which can enhance the second-order susceptibility observed in nitride quantum wells.[49] In InGaN/GaN quantum wells, a value of $\chi^{(2)}$ one order of magnitude larger than the intrinsic value for GaN was obtained.

## V. CONCLUSIONS

We have experimentally demonstrated giant enhancement of the SHG by a factor of 5000 in a one-dimensional GaN PhC when the fundamental and the SH fields are phase matched with the second and the fourth lowest resonant modes, respectively. We interpret this enhancement as being primarily due to the simultaneous confinement of both fundamental and SH fields which occur when the QPM conditions are fulfilled. The angular configuration at the maximum SHG point agrees closely with QPM conditions determined beforehand from either the experimental or the calculated EFS at 791 and 395.5 nm.

To our knowledge, this is the first demonstration of the new possibilities offered by the use of PhCs to provide giant SHG in GaN. The enhancements have clearly not yet been optimized. Optimization will require a careful search in a parameter space that includes the layer and substrate refractive indices, the layer thickness—and the photonic crystal periodicity and filling factor, as well as the angle of incidence.

## ACKNOWLEDGMENTS

The authors would like to acknowledge R. M. De La Rue, DEEE University of Glasgow, for helpful suggestions. This work was partially supported by Région Languedoc-Roussillon through a BDI Grant.

*Electronic mail: coquillat@ges.univ-montp2.fr

[1] J. D. Jouannopoulos, R. R. Meade, and J. N. Winn, *Photonic Crystals, Molding the Flow of Light* (Princeton University Press, Princeton, NJ, 1995).

[2] *Photonic Crystals and Light Localization in the 21st Century*, edited by C. M. Soukoulis (Kluwer Academic, Dordrecht, 2001).

[3] T. F. Krauss and R. M. De La Rue, Prog. Quantum Electron. **23**, 51 (1999).

[4] For recent review see Focus Issue Nonlinear Optics and Photonic Crystals (NOPC), edited by C. M. Bowden and A. M. Zheltikov, J. Opt. Soc. Am. B **19**, 1961 (2002).

[5] J. A. Armstrong, N. Bloembergen, J. Ducuing, and P. S. Pershan, Phys. Rev. **127**, 1918 (1962).

[6] P. A. Franken and J. F. Ward, Rev. Mod. Phys. **35**, 23 (1963).

[7] J. P. van der Ziel and M. Ilegems, Appl. Phys. Lett. **28**, 437 (1976).

[8] M. Scalora, M. J. Bloemer, A. S. Manka, J. P. Dowling, C. M. Bowden, R. Viswanathan, and J. W. Haus, Phys. Rev. A **56**, 3166 (1997).

[9] M. Centini, C. Sibilia, M. Scalora, G. D'Aguanno, M. Bertolotti, M. J. Bloemer, C. M. Bowden, and I. Nefedov, Phys. Rev. E **60**, 4891 (1999).

[10] R. Reinisch and M. Nevière, Phys. Rev. B **26**, 5987 (1982).
[11] M. M. Fejer, G. A. Magel, D. H. Jundt, and R. L. Bayer, IEEE J. Quantum. Electron. **28**, 2631 (1992).
[12] A. V. Balakin, V. A. Bushuev, B. I. Mantsyzov, I. A. Ozheredov, E. V. Petrov, A. P. Shkurinov, P. Masselin, and G. Mouret, Phys. Rev. E **63**, 046609 (2001).
[13] Y. Dumeige, P. Vidakovic, S. Sauvage, I. Sagnes, J. A. Levenson, C. Sibilia, M. Centini, G. D'Aguanno, and M. Scalora, Appl. Phys. Lett. **78**, 3021 (2001).
[14] Y. Dumeige, I. Sagnes, P. Monnier, P. Vidakovic, I. Abram, C. Méríadec, and A. Levenson, Phys. Rev. Lett. **89**, 043901 (2002).
[15] S. G. Tikhodeev, A. L. Yablonskii, E. A. Muljarov, N. A. Gippius, and T. Ishihara, Phys. Rev. B **66**, 045102 (2002).
[16] M. Galli, M. Agio, L. Atzeni, D. Bajoni, G. Guizzeti, L. Businaro, E. Di. Fabrizio, F. Romanato, and A. Passaseo, Eur. Phys. J. B **27**, 79 (2002).
[17] A. R. Cowan and J. F. Young, Phys. Rev. B **65**, 085106 (2002).
[18] A. M. Malvezzi, F. Cattaneo, G. Vecchi, M. Falasconi, G. Guizzetti, L. C. Andreani, F. Romanato, L. Businaro, E. Di Fabrizio, A. Passaseo, and M. De Vittorio, J. Opt. Soc. Am. B **19**, 2122 (2002).
[19] J. Miragliotta and D. K. Wickenden, Phys. Rev. B **53**, 1388 (1996).
[20] I. M. Tiginyanu, I. V. Kravetsky, D. Pavlidis, A. Eisenbach, R. Hildebrandt, G. Marowsky, and H. Hartnagel, MRS Internet J. Nitride Semicond. Res. **5S1**, W11.52 (2000).
[21] D. Coquillat, S. Murad, A. Ribayrol, C. Smith, R. De La Rue, C. Wilkinson, O. Briot, and R. L. Aulombard, ICSCIII-N'97, Stockholm, Mater. Sci. Forum **264–268**, 1403 (1998).
[22] D. Coquillat, A. Ribayrol, R. M. De La Rue, M. Le Vassor d'Yerville, D. Cassagne, and J. P. Albert, Appl. Phys. B: Lasers Opt. **73**, 1 (2001).
[23] D. Peyrade, J. Torres, D. Coquillat, R. Legros, J. P. Lascaray, Y. Chen, L. Manin-Ferlazzo, S. Ruffenach, O. Briot, M. Le Vassor d'Yerville, E. Centeno, D. Cassagne, and J. P. Albert, Physica E (in press).
[24] A. Ribayrol, D. Coquillat, R. M. De La Rue, S. K. Murad, C. D. W. Wilkinson, P. Girard, O. Briot, and R. L. Aulombard, Mater. Sci. Eng., B **59**, 335 (1999).
[25] D. Coquillat, A. Ribayrol, R. M. De La Rue, P. Girard, O. Briot, R. L. Aulombard, D. Cassagne, and C. Jouanin, Phys. Status Solidi B **216**, 669 (1999).
[26] P. St. J. Russell, T. A. Birks, and F. D. Lloyd-Lucas, in *Confined Electrons and Photons*, edited by E. Burstein and C. Weisbuch (Plenum, New York, 1995), 585 pp.
[27] H. Kosaka, T. Kawashima, A. Tomita, M. Notomi, T. Tamamura, T. Sato, and S. Kawakami, Phys. Rev. B **58**, R10 096 (1998).
[28] H. Kosaka, T. Kawashima, A. Tomita, M. Notomi, T. Tamamura, T. Sato, and S. Kawakami, Appl. Phys. Lett. **74**, 1370 (1999).
[29] H. Kosaka, T. Kawashima, A. Tomita, M. Notomi, T. Tamamura, T. Sato, and S. Kawakami, Appl. Phys. Lett. **74**, 1212 (1999).
[30] H. Kosaka, A. Tomita, T. Kawashima, T. Sato, and S. Kawakami, Phys. Rev. B **62**, 1477 (2000).
[31] B. Gralak, S. Enoch, and G. Tayeb, J. Opt. Soc. Am. A **17**, 1012 (2000).
[32] M. Notomi, T. Tamamura, Y. Ohtera, O. Hanaizumi, and S. Kawakami, Phys. Rev. B **61**, 7165 (2000).
[33] M. Notomi, Phys. Rev. B **62**, 10 696 (2000).
[34] E. Silvestre, J. M. Pottage, St. J. Russell, and P. J. Roberts, Appl. Phys. Lett. **77**, 942 (2000).
[35] J. M. Pottage, E. Silvestre, and P. St. Russell, J. Opt. Soc. Am. A **18**, 442 (2001).
[36] M. C. Netti, A. Harris, J. J. Baumberg, D. M. Whittaker, M. B. D. Charlton, M. E. Zoorob, and G. J. Parker, Phys. Rev. Lett. **86**, 1526 (2001).
[37] T. Baba and T. Matsumoto, Appl. Phys. Lett. **81**, 2325 (2002).
[38] D. M. Whittaker and I. S. Culshaw, Phys. Rev. B **60**, 2610 (1999).
[39] D. Peyrade, Y. Chen, L. Manin-Ferlazzo, A. Lebib, N. Grandjean, D. Coquillat, R. Legros, and J. P. Lascaray, Microelectron. Eng. **57/58**, 843 (2001).
[40] P. M. Lundquist, H. C. Ong, W. P. Lin, R. P. H. Chang, J. B. Ketterson, and G. K. Wong, Appl. Phys. Lett. **67**, 2919 (1995).
[41] G. D'Aguanno, M. Centini, M. Scalora, C. Sibilia, Y. Dumeige, P. Vidakovic, J. A. Levenson, M. J. Bloemer, C. M. Bowden, J. W. Haus, and M. Bertolotti, Phys. Rev. E **64**, 016609 (2001).
[42] V. Astratov, R. Stevenson, S. Culshaw, D. Whittaker, M. Skolnick, T. F. Krauss, and R. M. De La Rue, Appl. Phys. Lett. **77**, 178 (2000).
[43] V. N. Astratov, D. M. Whittaker, I. S. Culshaw, R. M. Stevenson, M. S. Skolnick, T. F. Krauss, and R. M. De La Rue, Phys. Rev. B **60**, R16 255 (1999).
[44] W. L. Barnes, T. W. Preist, S. C. Kitson, and J. R. Sambles, Phys. Rev. B **54**, 6227 (1996).
[45] V. Pacradouni, W. J. Mandeville, A. R. Cowan, P. Paddon, J. F. Young, and S. R. Johnson, Phys. Rev. B **62**, 4204 (2000).
[46] M. Galli, M. Agio, L. C. Andreani, M. Belotti, G. Guizzetti, F. Marabelli, M. Patrini, P. Bettotti, L. Dal Negro, Z. Gaburro, L. Pavesi, A. Lui, and P. Bellutti, Phys. Rev. B **65**, 113111(R) (2002).
[47] J. B. Harris, T. W. Preist, E. L. Wood, and J. R. Sambles, J. Opt. Soc. Am. A **13**, 803 (1996).
[48] D. Cassagne, C. Jouanin, and D. Bertho, Phys. Rev. B **53**, 7134 (1996).
[49] H. Schmidt, A. C. Abare, J. E. Bowers, S. P. Denbaars, and A. Imamoğlu, Appl. Phys. Lett. **75**, 3611 (1999).